

Pressure Recovery Discharge Configurations for an Induced Draught Axial Flow Fan

G. M. Bekker^a, C. J. Meyer^b, S. J. van der Spuy^c

Received 21 September 2021, in revised form 27 December 2021 and accepted 17 January 2022

Abstract: This study investigates the potential gains in operating volume flow rate and static efficiency of an induced draught axial flow fan system. These gains are achieved through pressure recovery, i.e. the conversion of dynamic pressure at the fan exit into static pressure. Pressure recovery is achieved using downstream diffusers, stator blade rows, and combinations of these. Three different diffuser lengths are considered. Of the shortest diffusers, a conical diffuser increases the operating volume flow rate by 3.2 % and the fan static efficiency by 9.8 % (absolute). A longer conical diffuser increases it by 3.9 % and 11.9 %, respectively. Of the longest diffusers, an annular diffuser increases the flow rate by 5.5 % and the fan static efficiency by 16.8 %.

Additional keywords: Pressure recovery, axial flow fan, induced draught, diffuser, stator.

Nomenclature

Roman

A	Area [m ²]
AR	Diffuser area ratio
a	Curve fitting coefficient [kg/m ⁷]
C_D	Drag coefficient
C_L	Lift coefficient
d	Diameter [m]
F	Force [N]
K_{dif}	Diffuser total pressure loss coefficient
K_{rec}	Pressure recovery coefficient
K_{rec}^*	Pressure recovery coefficient as per Bekker <i>et al.</i> [1]
k	Turbulence kinetic energy [m ² /s ²]
l	Length [m]
P_F	Fan power consumption [W]
p	Pressure [Pa]
r	Radius [m]
t	Actuator disc thickness [m]
V, \dot{V}	Volume [m ³]; and volume flow rate [m ³ /s]
v	Velocity [m/s]
y	Wall-normal distance [m]
y^+	Sublayer-scaled wall-normal distance

Greek

α_e	Kinetic energy flux correction factor
β	Relative flow angle [deg]
β_1	Turbulence model constant, 0.075
Δ, δ	Difference; and small difference
η	Efficiency [%]
θ	Diffuser half-wall angle [deg]
ν	Kinematic molecular viscosity [m ² /s]
ρ	Density [kg/m ³]
σ	Blade solidity
ω	Turbulence specific dissipation rate [s ⁻¹]

Subscripts

des	Design point
dif	Diffuser
down	Downstream
dump	Dump representing the open atmosphere
e	Exit (fan or diffuser outlet)
F	Fan
FC	Fan casing
F/dif	Fan-diffuser unit
F/difs	Fan-diffuser static
FH	Fan hub
Fs	Fan static
Ft	Fan total
HE	Heat exchanger
i	Inlet or inner diffuser wall
inlet	Inlet boundary
max	Maximum
o	Outlet or outer diffuser wall
op	Operating point
R	Relative
s	Static
t	Total (or stagnation)
up	Upstream
x, θ	Axial and tangential directions
∞	Atmospheric conditions

Abbreviations

ACC	Air-cooled condenser
ADM	Actuator disc model
CFD	Computational fluid dynamics
DILU	Diagonal-based incomplete LU preconditioner
EADM	Extended actuator disc model
GAMG	Geometric-algebraic multi-grid solver
PBiCG	Preconditioned bi-conjugate gradient solver
SIMPLE	Semi-implicit method for pressure-linked equations

1 Introduction

This research focuses on improving the performance of an axial flow fan to be used in an induced draught air-cooled condenser (ACC). Such ACCs employ large arrays of axial

- Department of Mechanical and Mechatronic Engineering, Stellenbosch University, South Africa. E-mail: 17732956@sun.ac.za
- Associate Professor. Department of Mechanical and Mechatronic Engineering, Stellenbosch University, South Africa. E-mail: cjmeyer@sun.ac.za
- SAIMechE Member, Professor. Department of Mechanical and Mechatronic Engineering, Stellenbosch University, South Africa. E-mail: sjvdspuy@sun.ac.za

flow fans to draw air through heat exchanger bundles in order to condense the process fluid inside the heat exchanger tubes.

The improvement in fan performance was achieved through pressure recovery. Pressure recovery refers to the conversion of dynamic pressure at the fan outlet into static pressure. The effect of pressure recovery is to increase the effective fan static pressure rise. In an ACC fan unit, the fan curve and resistance curve then intersect at a higher fan static pressure and airflow rate. The increased airflow rate through the heat exchangers allows for higher heat rejection rates from the process fluid to the air. The increased fan static pressures also translate to improved operating fan static efficiencies.

Bekker *et al.* [1] reported significant gains in fan performance due to pressure recovery. They examined six different types of discharge configurations for an axial flow fan: For the first type, the fan was followed by a stator blade row. Conical diffusers comprised the second type. The third type combined the stator and conical diffusers so that the stator followed the fan and the diffusers followed the stator blade row. The fourth and fifth types involved annular diffusers with and without a stator blade row between the fan and diffusers. The sixth and final outlet configuration had a stator blade row fitted at the outlet of an annular diffuser.

Bekker *et al.* [1] used the M-fan for their study. This fan was designed by Wilkinson *et al.* [2] to be used in modern ACCs. Table 1 summarises the attributes of the M-fan along with its performance characteristics at its design flow rate.

Table 1: Specifications and performance characteristics of the M-fan at a reference density of $\rho = 1.2 \text{ kg/m}^3$.

Attribute	Value or description
Diameter	24 ft (7.315 m)
Number of blades	8
Hub-to-tip ratio	0.29
Blade root setting angle	34°
Mean chord length	0.841 m
Blade profile	Optimised from NASA-LS
Rotational speed	151 rpm
Design flow rate	333 m ³ /s
Fan static pressure rise	115 Pa
Fan power consumption	64.24 kW
Fan static efficiency	59.4 %

The current study expands on the work of Bekker *et al.* [1]. The same discharge configurations are considered for the same axial flow fan. The theory and modelling strategies outlined in Bekker *et al.* [1] also apply here. However, Bekker *et al.* [1] investigated only a single diffuser length equal to the fan diameter, i.e. 7.315 m. They also used conservative axial clearances between the fan, stator rows, and diffusers. The overall length of the discharge configurations considered by Bekker *et al.* [1] ranged between 9.24 and 10.53 metres. Such lengths, however, are considered impractical.

Furthermore, as per BS EN ISO 5801 [3], Bekker *et al.* [1] assumed the static pressure at the fan outlet to be equal to atmospheric pressure. However, Bekker *et al.* [4] established that the static pressure at the fan outlet is, in fact, lower than atmospheric pressure. The result is that the

pressure recovery coefficients presented in Bekker *et al.* [1] are optimistic.

Consequently, shorter discharge diffusers were investigated in the current study. Less conservative axial clearances between turbomachinery blading and diffusers were also used. Additionally, pressure recovery coefficients were calculated using the more conservative formula suggested by Bekker *et al.* [4].

Two shorter diffuser lengths equal to 40 % and 20 % of the fan diameter were considered. That is, 2.926 and 1.463 metres, respectively. Kröger [5] portrays a diffuser of a length equal to $l_{\text{dif}} = 0.4d_F$ (where d_F is the fan diameter) as a “practical diffuser”.

At the start of the paper, pressure recovery theory is revised to illustrate how pressure recovery influences axial flow fan performance in induced draught systems. Detail pertaining to the numerical simulation approach follows. Pressure recovery coefficients obtained with different discharge configurations for the M-fan are presented next. These were obtained at the design flow rate of the fan. The configurations producing the highest pressure recoveries at the design flow rate were investigated further at off-design flow rates. Finally, the pressure recovery data of the most promising discharge configurations of each length were added to the performance characteristics of the M-fan. This allows for comparison between the fan-diffuser and M-fan characteristics. A summary of the main findings concludes the paper.

2 Pressure Recovery Theory

Figure 1 depicts a fan system representative of an induced draught ACC. The draught equation for this system is given by (see the appendix for a detailed derivation)

$$\Delta p_{F_s} + \alpha_{eFC} \rho v_{FC}^2 / 2 = \Delta p_{HE} + K_{\text{dif}} \rho v_{FC}^2 / 2 + \alpha_{e\text{dif}} \rho v_{\text{dif}}^2 / 2 \quad (1)$$

On the left-hand side of equation (1), energy is supplied to the system by the axial flow fan. From left to right, Δp_{F_s} is the fan static pressure rise, α_{eFC} is the kinetic energy flux factor at the fan exit, ρ is the air density, and $v_{FC} = \dot{V}/A_{FC}$ is the mean axial velocity through the fan casing. The terms on the right-hand side of equation (1) represent the energy dissipated as air passes through the system. From the left again, Δp_{HE} represents the static pressure loss due to the heat exchanger and K_{dif} is the total pressure loss coefficient of the

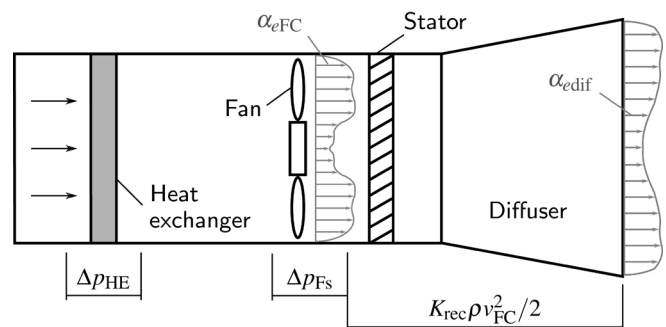


Figure 1: Schematic of an induced draught fan system.

diffuser. At the outlet of the diffuser, α_{edif} is the kinetic energy flux factor and $v_{dif} = \dot{V}/A_{dif}$ is the mean axial velocity.

According to Kröger [5], α_{eFC} , K_{dif} and α_{edif} are normally unknown and troublesome to measure. Therefore, Bekker *et al.* [1] moved these terms to the left-hand side of equation (1) and grouped them to form a pressure recovery coefficient. This coefficient is obtained by normalising this group of terms with the mean axial dynamic pressure through the fan casing so that

$$K_{rec} := \alpha_{eFC} - \alpha_{edif}(AR)^{-2} - K_{dif} \quad (2)$$

where $AR = A_{dif}/A_{FC}$ is the area ratio of the diffuser.

Substituting equation (2) into equation (1) simplifies the draught equation to

$$\Delta p_{Fs} + K_{rec}\rho v_{FC}^2/2 = \Delta p_{HE} \quad (3)$$

If $K_{rec} = \alpha_{eFC}$, the effective fan pressure rise would equal the fan total pressure rise, i.e. $\Delta p_{Ft} = \Delta p_{Fs} + \alpha_{eFC}\rho v_{FC}^2/2$. This would result in the highest operating flow rate theoretically possible, \dot{V}_{max} . However, continuity requires that $\alpha_{edif} \geq 1$ and diffuser stall limits AR . Furthermore, viscous and local losses in the diffuser translate to $K_{dif} > 0$.

The static pressure characteristics of the fan-diffuser unit, $\Delta p_{F/difs} = \Delta p_{Fs} + K_{rec}\rho v_{FC}^2/2$, will therefore be higher than the static pressure characteristics of the fan but lower than the fan's total pressure characteristics (see figure 2). Figure 2 further illustrates how pressure recovery shifts the operating point of the fan system to a higher operating volume flow rate, \dot{V}_{op} , compared to the initial design flow rate, \dot{V}_{des} .

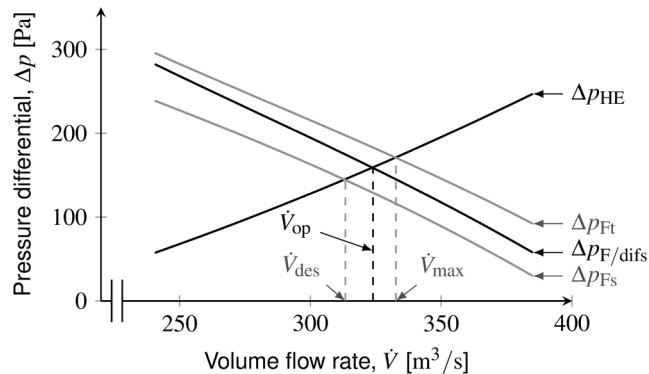


Figure 2: Influence of pressure recovery on the pressure characteristics of the fan. Adapted from [1].

Induced draught ACCs fitted with appropriate discharge configurations could therefore operate at flow rates that are higher than the design flow rate. Owing to the increased mass flow rate of air through the heat exchangers, the ACC will be capable of transferring more heat from the process fluid to the atmosphere.

3 Numerical Approach

Because of the large physical size of ACC fans, full-scale testing is considered impractical. Furthermore, the number of

discharge configurations that had to be tested was significant. By means of computational fluid dynamics (CFD), it was possible to obtain pressure recovery data for a total of 548 outlet configurations for the M-fan. Computations were performed employing the open-source CFD code, OpenFOAM 5.0.

3.1 Numerical validation

Prior to the simulation of the different discharge configurations, the CFD approach was validated against the experimental data of Clausen *et al.* [6] for swirling flow in a conical diffuser. Full details of the validation study are available in Bekker *et al.* [1].

Bekker *et al.* [1] tested various high- and low-Reynolds-number turbulence models and found that the wall-integrated $k-\omega$ model of Wilcox [7] produced reasonable results. Since it was found that results were sensitive to the specified inlet turbulence quantities, it was decided to use profiles for turbulence quantities that Wilkinson [8] measured downstream of the M-fan. Furthermore, Bekker *et al.* [1] found that steady-state simulations performed on two-dimensional axisymmetric meshes produced results on par with transient and three-dimensional simulations.

3.2 Computational domain and mesh

The computational domain for one of the more complex discharge configurations for the M-fan is depicted in figure 3a. It is the domain that was used for the annular diffusers fitted with a stator row at their inlets.

Block-structured meshes comprising of hexahedral cells were generated using OpenFOAM's blockMesh utility (see figure 3b). The meshes were wedge-shaped, consisting of a single computational cell in the tangential direction. The

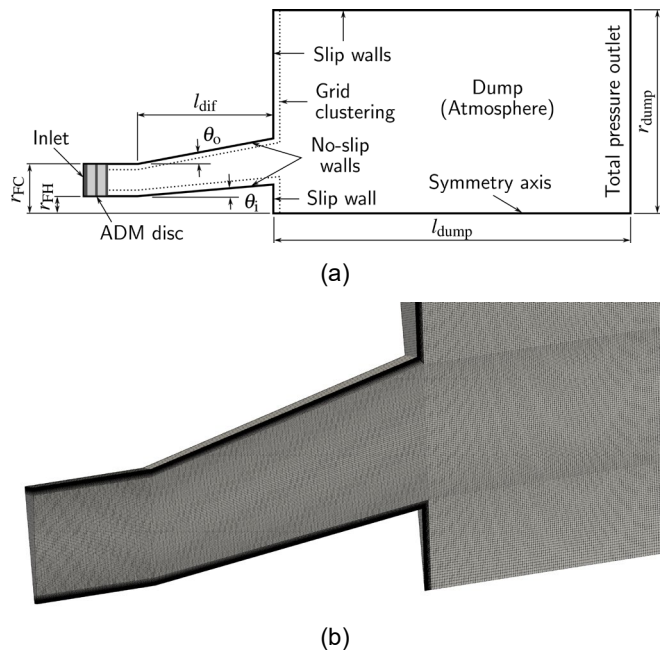


Figure 3: (a) Computational domain with boundary conditions and (b) computational mesh for annular diffusers fitted with a stator row at their inlets. The domain is wedge-shaped with a wedge angle of five degrees.

wedge angle was set to five degrees, as recommended by Greenshields [9] for axisymmetric flow problems. Grid-clustering at solid surfaces facilitated integration through the boundary layer. The width of such a clustered zone was 5 % of the fan diameter and had a high degree of grading towards the wall. The grading allowed for $y^+ \sim 1$ at the walls and a smooth transition with the inner mesh.

3.3 Boundary conditions

The inlet of the domain was located at one-half mean fan-blade chord length downstream of the M-fan. The fan itself was thus not modelled. Instead, fixed velocity and turbulence profiles at the fan outlet were used to specify the inlet boundary conditions. These profiles were obtained from Wilkinson [8] for flow rates ranging from 260 to 380 m³/s. These profiles were computed using a three-dimensional periodic fan model with no tip clearance.

It is reasonable to assume that downstream stator blade rows or diffusers will not significantly alter the flow profiles exiting the fan: Terzis *et al.* [10] found that outlet guide vanes did not alter the velocity profiles at the outlet of a small fan. And Bekker *et al.* [4] obtained similar velocity profiles at the outlet of the M-fan with or without discharge diffusers. Along with the velocity and turbulence profiles specified at the inlet, a zero-gradient condition was assigned to pressure.

The remainder of the boundary conditions are displayed in figure 3: At no-slip surfaces, $k = 0$, $\omega = 6\nu/(\beta_1 y^2)$ [11], and $\nabla p = 0$ were used. A fixed total pressure of zero was assigned to the outlet boundary along with zero gradients for velocity and turbulence quantities. In the case of reverse flow at the outlet, velocity was calculated from the flux in the boundary-normal direction. Wedge boundaries were specified for the axisymmetric planes. These function as cyclic boundaries for two-dimensional axisymmetric problems in OpenFOAM. A symmetry condition was applied to the axisymmetric axis of the domain.

3.4 Numerical solver settings

Simulations devoid of stator blade rows employed a steady-state solver for incompressible flows with turbulence, i.e. the `simpleFoam` solver. When stator blade rows required modelling, the extended actuator disc model (EADM) of Van der Spuy [12] was used. Engelbrecht [13] incorporated this model into the `buoyantBoussinesqSimpleFoam` solver of OpenFOAM. Both mentioned solvers employ the SIMPLE algorithm to solve the continuity and momentum equations. The following section provides more detail regarding the EADM.

Table 2 provides the discretisation schemes that were used for the gradient and divergence terms. The discretisation of Laplacian terms requires an interpolation scheme and a surface-normal gradient scheme. The former was achieved using linear interpolation from cell centres to face centres. The surface-normal gradients were discretised using a limited-corrected scheme with a relaxing coefficient of 0.33.

The linear solvers that were used for each governing variable are listed in table 3. This table also contains the under-relaxation factors that were used for the iterative solution procedure.

The kinematic viscosity and density of air at 20 °C were used, i.e. $\nu \approx 1.5 \times 10^{-5}$ and $\rho \approx 1.2 \text{ kg/m}^3$, respectively. Solutions were deemed converged after the static pressure at the domain inlet settled to a constant value and the scaled residuals reduced to 10^{-4} or lower.

Table 2: Numerical discretisation schemes.

Governing variable	Gradient scheme	Divergence scheme
p	2 nd -order linear	–
\vec{v}	2 nd -order linear	Bounded 2 nd -order linear-upwind
k, ω	2 nd -order linear	Bounded 1 st -order upwind

Table 3: Linear solver settings and under-relaxation factors.

Governing variable	Linear solver	Smoother or preconditioner	Under-relaxation
p	GAMG	GaussSeidel	0.2
\vec{v}	PBiCGStab	DILU	0.6
k, ω	PBiCGStab	DILU	0.7

3.5 Sensitivity studies

The computational mesh density was increased up to a point where the computed pressure recovery coefficient changed by less than two per cent compared to the result obtained with the previous coarser mesh. In addition, the velocity profiles at the outlet of the discharge configurations using successively refined meshes had to be near identical before considered grid-independent.

For each type of fan-outlet configuration, the sensitivity to the size of the discharge dump that represented the open atmosphere was investigated (see figure 3). The dump size (r_{dump} and l_{dump}) was increased up to a point where the pressure recovery and velocity profiles no longer changed.

4 Stator Modelling

Stator blade rows were modelled using the extended actuator disc model (EADM) of Van der Spuy [12]. This model employs isolated aerofoil data to compute the force a fan blade would exert on air. The force is introduced into the momentum equation through a source term. The axial component of the source term is calculated as

$$\frac{\delta F_x}{\delta V} = \frac{1}{2} v_R^2 \frac{\sigma}{t} (C_L \cos \beta - C_D \sin \beta) \quad (4)$$

and the tangential component as

$$\frac{\delta F_\theta}{\delta V} = \frac{1}{2} v_R^2 \frac{\sigma}{t} (C_L \sin \beta + C_D \cos \beta) \quad (5)$$

In the above equations, v_R and β are the relative velocity vector and flow angle, σ is the blade solidity, and t is the thickness of the actuator disc. The lift and drag coefficients, C_L and C_D , are obtained from isolated aerofoil data.

In order to compute the source terms described by equations (4) and (5), the model requires the blade chord and

stagger angle distributions. These distributions were computed using the isolated aerofoil design method outlined in Louw *et al.* [14].

A nine-bladed stator row with the blade angle and chord length distributions in figure 4 was capable of removing all the swirl exiting the M-fan at the design flow rate. As recommended by Wallis [15], the stator was located at a half mean rotor chord length downstream of the fan.

For the discharge configurations where stator blade rows were installed at the outlet of annular diffusers, new stator rows had to be designed. In order to obtain realistic chord lengths, these stator rows required 13 blades and could remove only ~50 % of the swirl exiting the annular diffusers.

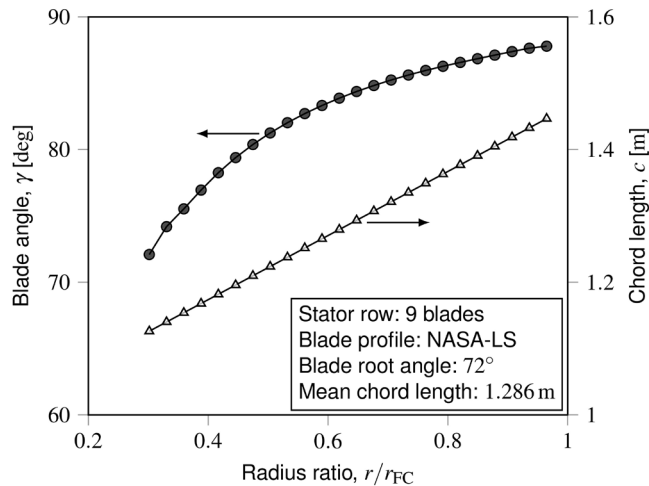


Figure 4: Blade angle and chord length distributions of the stator blade row at the outlet of the M-fan. The blade angle is measured from the tangential direction to the chord line of the blade.

5 M-fan Discharge Configurations

Similar to Bekker *et al.* [1], various discharge configurations were investigated for the M-fan. The aim was to find configurations producing high pressure recovery coefficients at both design and off-design conditions. After identifying the most promising discharge configurations, their pressure recovery data were added to the characteristics of the M-fan. The characteristics of the M-fan and fan-diffuser units could then be compared to quantify the gains in performance due to pressure recovery.

5.1 Calculation of pressure recovery

Bekker *et al.* [1] computed the pressure recovery coefficient of a discharge configuration as

$$K_{rec}^* = \frac{p_\infty - \bar{p}_{inlet}}{\rho v_{FC}^2 / 2} \tag{6}$$

where \bar{p}_{inlet} is the area-weighted static pressure measured at the inlet of the computational domain and p_∞ is equal to atmospheric pressure. BS EN ISO 5801 [3] stipulates that the static pressure at the fan outlet in equation (6) should be assumed to be equal to atmospheric pressure. In other words, without any discharge configuration recovering pressure, $\bar{p}_{inlet} = p_\infty$ should be true so that $K_{rec}^* = 0$.

Bekker *et al.* [4], however, established that $\bar{p}_{inlet} < p_\infty$ even though no downstream stator blade row or diffuser was present. For the fan on its own, equation (6) thus erroneously yields $K_{rec}^* > 0$. Bekker *et al.* [4] therefore analysed the fan exit region without any discharge configuration. The same velocity and turbulence profiles of Wilkinson [8] were utilised to obtain the average static pressure at the fan outlet at different flow rates. They then corrected equation (6) as follows:

$$K_{rec} = \frac{p_\infty - \bar{p}_{e,F/dif}}{\rho v_{FC}^2 / 2} - \frac{p_\infty - \bar{p}_{e,F}}{\rho v_{FC}^2 / 2} = \frac{\bar{p}_{e,F} - \bar{p}_{e,F/dif}}{\rho v_{FC}^2 / 2} \tag{7}$$

where $\bar{p}_{e,F}$ is the area-weighted static pressure measured at the domain inlet (which corresponds to the fan outlet) without any discharge configuration and $\bar{p}_{e,F/dif}$ is measured in the same manner but with a discharge configuration. Bekker *et al.* [4] demonstrated that equation (7) is more conservative than equation (6), especially at lower off-design flow rates. The pressure recovery coefficients presented in the sections to follow were computed using equation (7).

5.2 Pressure recovery at design conditions

Parametric studies were performed at the fan’s design flow rate of 333 m³/s. For each diffuser length, the area ratio was varied by changing the divergence angle of the diffuser.

For the conical diffusers of length $l_{dif} = d_F$, the half-wall angle (angle between the axial direction and diffuser wall) was varied within the range of $0^\circ \leq \theta \leq 20^\circ$ in increments of one degree. Half-wall angles of $0^\circ \leq \theta \leq 25^\circ$ were tested for conical diffusers of length $l_{dif} = 0.4d_F$. And the shortest diffusers, $l_{dif} = 0.2d_F$, were tested in a narrower range of $8^\circ \leq \theta \leq 24^\circ$.

Figure 5 depicts the pressure recovery data for the different area ratios that were tested. These results were obtained with no stator blade row present. The same procedure was followed for the conical diffusers with a stator row located between the fan outlet and diffuser inlet.

For the configurations involving annular diffusers, numerous combinations of inner and outer half-wall angles were tested. The inner half-wall angle was varied within the range of $0^\circ \leq \theta_i \leq 30^\circ$ in increments of two degrees for the longest diffusers, i.e. $l_{dif} = d_F$. A range of outer half-wall angles, θ_o , was tested for each of these inner half-wall angles. The $l_{dif} = 0.4d_F$ diffusers were tested for $-10^\circ \leq \theta_i \leq 30^\circ$ in increments of two degrees. Finally, the $l_{dif} = 0.2d_F$ diffusers were tested in larger increments of four degrees in the range of $-20^\circ \leq \theta_i \leq 8^\circ$.

Evidently, considerably more simulations were required to obtain the annular diffuser geometry producing the highest pressure recovery coefficient for each diffuser length compared to the conical diffuser cases. That is, similar to figure 5, a pressure recovery coefficient versus area ratio graph could be constructed for each inner half-wall angle that was investigated.

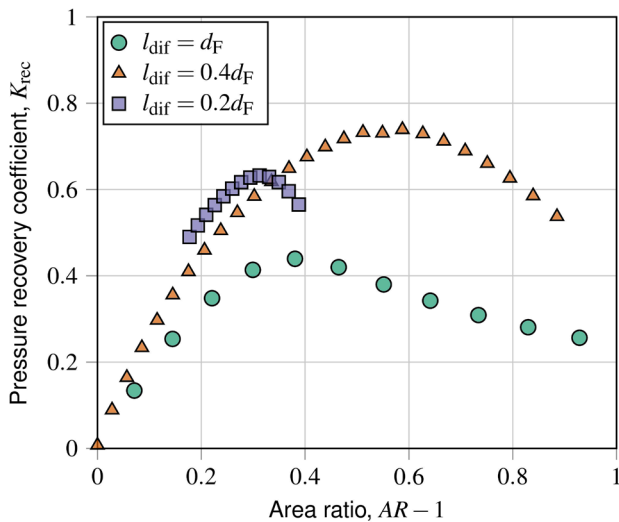


Figure 5: Variation of pressure recovery coefficient with area ratio for different lengths of conical diffusers. In this case, no stator blade row was present.

Following the above procedure, it was possible to identify the most promising diffuser geometries for each type of discharge configuration. The geometries of the best performing diffusers for the M-fan at the design flow rate are summarised in tables 4 to 6.

Table 4: Diffusers of length $l_{dif} = d_F$ that produced the highest pressure recovery coefficients at the design flow rate. Reproduced from [1].

Diffuser arrangement	Half-wall angle
Conical	$\theta = 5^\circ$
Conical with stator at inlet	$\theta = 8^\circ$
Annular	$\theta_i = 22^\circ, \theta_o = 22^\circ$
Annular with stator at inlet	$\theta_i = 0^\circ, \theta_o = 14^\circ$
Annular with stator at outlet	$\theta_i = 22^\circ, \theta_o = 22^\circ$

Table 5: Diffusers of length $l_{dif} = 0.4d_F$ that produced the highest pressure recovery coefficients at the design flow rate.

Diffuser arrangement	Half-wall angle
Conical	$\theta = 16^\circ$
Conical with stator at inlet	$\theta = 15^\circ$
Annular	$\theta_i = -4^\circ, \theta_o = 16^\circ$
Annular with stator at inlet	$\theta_i = -6^\circ, \theta_o = 18^\circ$

Table 6: Diffusers of length $l_{dif} = 0.2d_F$ that produced the highest pressure recovery coefficients at the design flow rate.

Diffuser arrangement	Half-wall angle
Conical	$\theta = 20^\circ$
Conical with stator at inlet	$\theta = 20^\circ$
Annular	$\theta_i = -8^\circ, \theta_o = 20^\circ$
Annular with stator at inlet	$\theta_i = -12^\circ, \theta_o = 20^\circ$
Annular with stator at outlet	$\theta_i = -8^\circ, \theta_o = 20^\circ$

5.3 Pressure recovery under off-design conditions

The fans in ACCs often operate under off-design conditions: Louw *et al.* [16] found that the fans along the periphery of an induced draught ACC operate at slightly reduced flow rates due to flow separation along the sides of the ACC. They also reported that wind significantly reduces fan performance, especially in the wind-facing periphery units. Additionally, fouling could alter the operating point of a fan unit [5]. It is therefore important to determine how the different discharge configurations perform under off-design conditions.

The discharge configurations listed in tables 4 to 6 were evaluated at flow rates ranging from 260 to 380 m³/s. The pressure recovery coefficients obtained at these flow rates are presented in figures 6 to 8.

In every instance where a stator blade row is combined with a diffuser, the pressure recovery coefficient deteriorates significantly at lower off-design flow rates. The stator row on its own, however, does not exhibit such a large sensitivity to the flow rate. This suggests that the diffusers in the stator-diffuser combinations are responsible for the decline in pressure recovery at off-design flow rates.

With the stator row located between the fan outlet and diffuser inlet, the velocity profiles exiting the stator row at off-design flow rates are no longer conducive for diffuser performance. With stator rows at the annular diffuser outlets, the velocity profiles entering the stators are different from what the stators were designed for, as they were designed for the design flow rate. This results in increased losses in the stator row, which reduces pressure recovery. The discharge configurations featuring stator blade rows are therefore considered unsuccessful.

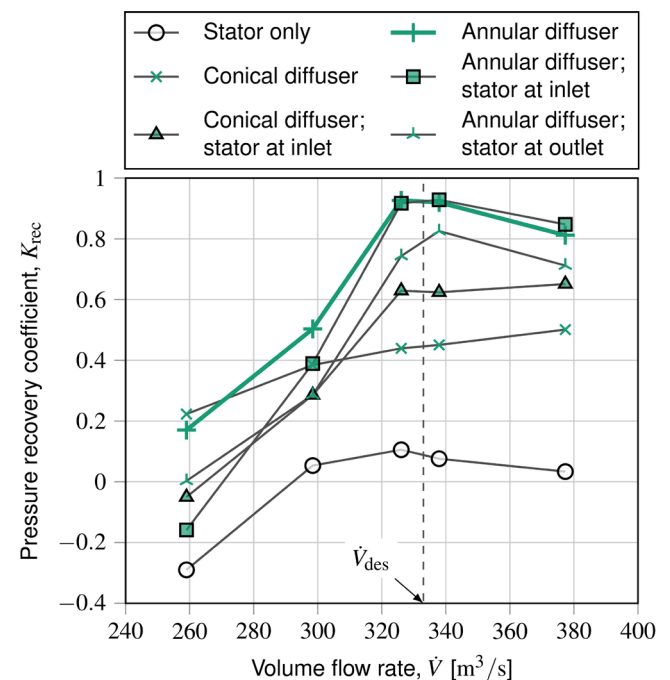


Figure 6: Variation of pressure recovery coefficient with volume flow rate for different outlet configurations. All diffusers had a length of $l_{dif} = d_F$.

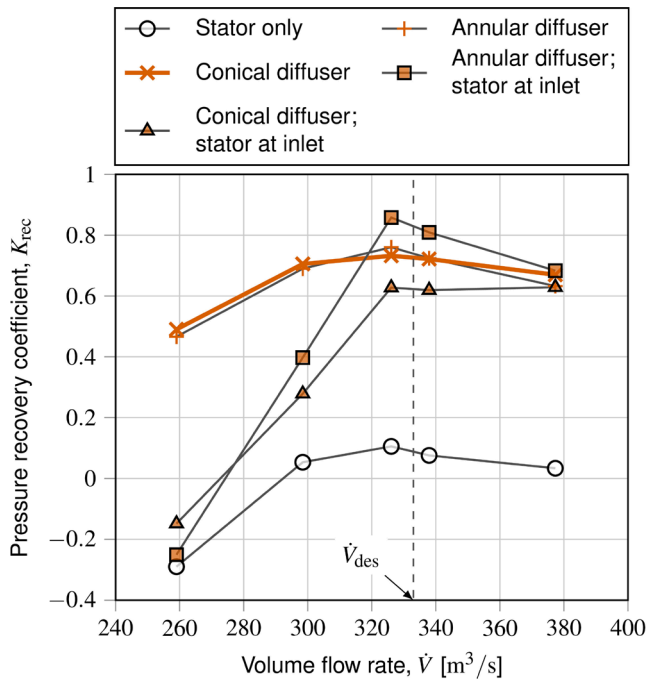


Figure 7: Variation of pressure recovery coefficient with volume flow rate for different outlet configurations. All diffusers had a length of $l_{dif} = 0.4d_F$.

Comparing the conical and annular diffuser results in figure 6 (without stator rows), the annular diffuser produces considerably higher pressure recovery coefficients. The annular diffuser with equiangular walls of 22° is therefore recommend for the $l_{dif} = d_F$ case.

The conical and annular diffusers for the shorter diffuser lengths yield essentially identical pressure recovery coefficients (see figures 7 and 8). Since conical diffusers

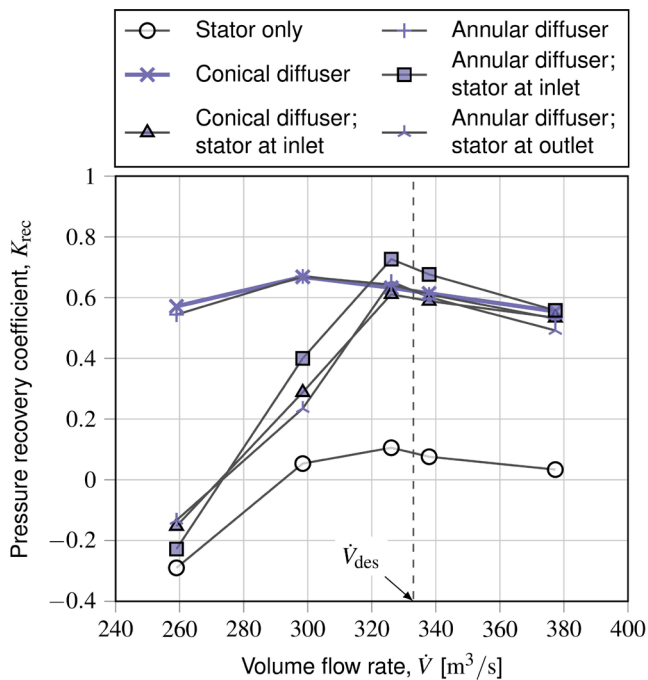


Figure 8: Variation of pressure recovery coefficient with volume flow rate for different outlet configurations. All diffusers had a length of $l_{dif} = 0.2d_F$.

require less material to manufacture and are simpler to install, they are recommended for the $l_{dif} = 0.2d_F$ and $l_{dif} = 0.4d_F$ lengths.

5.4 Effect of pressure recovery on fan performance characteristics

The pressure recovery data of the diffusers recommended in the previous section were added to the characteristics of the M-fan to obtain the combined fan-diffuser characteristics. For the $l_{dif} = d_F$ length, the 22° equiangular annular diffuser was recommended. For the $l_{dif} = 0.4d_F$ length, it was the conical diffuser with an included angle of $2\theta = 32^\circ$. For the $l_{dif} = 0.2d_F$ length, the $2\theta = 40^\circ$ conical diffuser was recommended.

Figure 9 depicts the static pressure characteristics. The fan characteristics were obtained from Wilkinson *et al.* [17], who used a periodic three-dimensional fan model with no tip clearance. A system curve representing the pressure drop of a typical heat exchanger was included in figure 9. It served to estimate the new operating points of the fan system after adding the diffusers. The pressure drop takes the general form of $\Delta p_{HE} = a\dot{V}^2$. The curve passes through the origin and the design point of 115 Pa at 333 m^3/s .

The static efficiency characteristics of the fan and fan-diffuser combinations are displayed in figure 10. The static efficiency of the fan was calculated as

$$\eta_{Fs} = \Delta p_{Fs} \dot{V} / P_F \tag{8}$$

where P_F is the shaft power supplied to the fan. For the fan-diffuser combinations, the efficiency was calculated with

$$\eta_{F/difs} = \Delta p_{F/difs} \dot{V} / P_F \tag{9}$$

where $\Delta p_{F/difs} = \Delta p_{Fs} + K_{rec} \rho v_{FC}^2 / 2$. Note that in both equations (8) and (9), the same fan power characteristics were used. Hence, it is assumed that the added diffusers do not alter the power characteristics. This is a reasonable assumption, as Bekker *et al.* [4] simulated scaled versions of these exact fan-diffuser combinations and found that the diffusers had no marked impact on the power characteristics.

The pressure recovery of the annular diffuser of length $l_{dif} = d_F$ increased the flow rate through the fan from 333 to 351 m^3/s . Thus, a relative increase of 5.5 %. The fan static efficiency rose from 59.4 % at the initial design point to 76.2 % at the new operating point. Thus, an absolute increase of 16.8 %.

The $l_{dif} = 0.4d_F$ conical diffuser shifted the operating flow rate to 346 m^3/s , which is a 3.9 % increase. The resulting operating fan static efficiency was 71.3 %, which is 11.9 % (absolute) higher than without the diffuser.

Finally, the $l_{dif} = 0.2d_F$ conical diffuser shifted the operating point to 123 Pa at 344 m^3/s , yielding a fan static efficiency of 69.2 %. The flow rate and static efficiency thus rose by 3.2 % (relative) and 9.8 % (absolute), respectively.

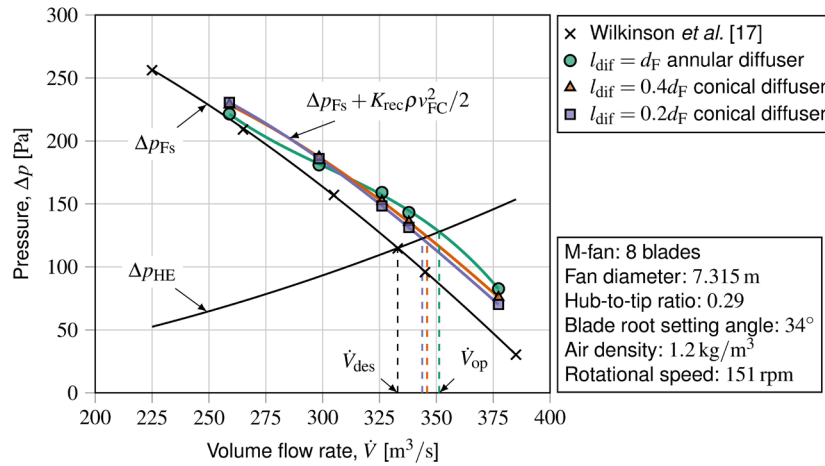


Figure 9: Effect of pressure recovery on the pressure characteristics of the M-fan.

6 Conclusions

This research followed on the work of Bekker *et al.* [1]. However, more practical (shorter) exhaust diffusers were also considered. Furthermore, pressure recovery coefficients were computed using the more conservative formula suggested by Bekker *et al.* [4].

The theory of pressure recovery for an axial flow fan in an induced draught system was revised. Pressure recovery data for various discharge configurations added to the M-fan were also provided. These configurations included combinations of conical and annular diffusers fitted with or without stator blade rows at their inlets. Cases with stator blade rows at the outlets of annular diffusers were also investigated. Three different diffuser lengths were considered for each type of discharge configuration.

The longest diffusers had a length equal to the fan diameter of 7.315 m. In this case, an annular diffuser with equiangular walls at 22° from the axial direction produced the highest pressure recovery coefficients over the considered range of flow rates. This diffuser increased the volume flow rate through the M-fan by 5.5 % relative to the initial design flow rate of 333 m³/s. The fan static efficiency also rose from 59.4 % to 76.2 %, i.e. an absolute increase of 16.8 %.

The mid-length diffusers had a length equal to 40 % of the fan diameter (i.e. 2.926 m). In this case, a conical diffuser

with a divergence angle of $2\theta = 32^\circ$ performed well over the considered range of flow rates. With this diffuser, the volume flow rate through the fan was 3.9 % higher than the initial design flow rate and the fan static efficiency was 11.9 % (absolute) higher at the new operating point.

The shortest diffusers were 1.463 m long, or 20 % of the length of the fan diameter. Of these configurations, a conical diffuser with a divergence angle of $2\theta = 40^\circ$ produced the most promising pressure recovery coefficients over the considered range of flow rates. The flow rate through the fan increased by 3.2 % relative to the initial design flow rate due to the added diffuser. The fan static efficiency rose by 9.8 %.

Appendix

The draught equation for the system in figure 1 is obtained by subtracting the total pressure far downstream of the system from the total pressure far upstream of the system, i.e.

$$\begin{aligned}
 p_{t,up} - p_{t,down} &= (p_{t,up} - p_{t,HE,i}) + (p_{t,HE,i} - p_{t,HE,o}) \\
 &+ (p_{t,F,i} - p_{t,F,o}) + (p_{t,dif,i} - p_{t,dif,o}) \\
 &+ (p_{t,dif,o} - p_{t,down}) = 0
 \end{aligned}
 \tag{10}$$

where $p_{t,HE,o} \approx p_{t,F,i}$ and $p_{t,F,o} \approx p_{t,dif,i}$ are assumed. In equation (10) and the equations to follow, subscripts “t” and

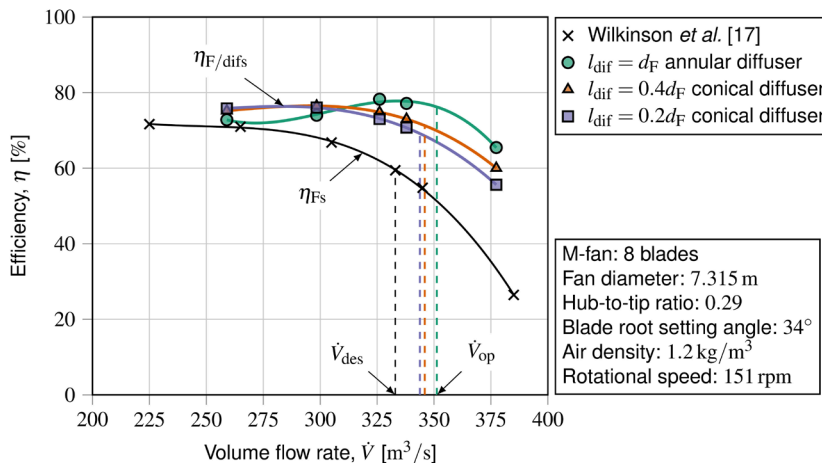


Figure 10: Effect of pressure recovery on the efficiency characteristics of the M-fan.

“s” denote total and static pressures, respectively. Subscripts “i” and “o” refer to the inlet and outlet sides of components, respectively. Furthermore, “F”, “HE” and “dif” subscripts denote fan, heat exchanger and diffuser, respectively.

The dynamic pressure at the inlet of the system is deemed negligible so that

$$p_{t,up} - p_{t,HE,i} \approx p_{\infty} - p_{s,HE,i} \approx 0 \quad (11)$$

Assuming that the dynamic pressures at the inlet and outlet of the heat exchanger are equal, the total pressure difference across the heat exchanger simplifies to

$$p_{t,HE,i} - p_{t,HE,o} = p_{s,HE,i} - p_{s,HE,o} = \Delta p_{HE} \quad (12)$$

In BS ISO 5801 [3], the fan total pressure is defined as $\Delta p_{Ft} = p_{t,F,o} - p_{t,F,i}$ and the fan static pressure is defined as $\Delta p_{Fs} = p_{s,F,o} - p_{t,F,i}$. The total pressure difference across the fan can therefore be expressed as

$$p_{t,F,i} - p_{t,F,o} = -\Delta p_{Ft} = -(\Delta p_{Fs} + \alpha_{eFC} \rho v_{FC}^2 / 2) \quad (13)$$

where $\alpha_{eFC} \rho v_{FC}^2 / 2$ is the dynamic pressure at the fan outlet.

The total pressure loss across the diffuser-stator discharge configuration is given by

$$p_{t,dif,i} - p_{t,dif,o} = K_{dif} \rho v_{FC}^2 / 2 \quad (14)$$

Finally, as per BS ISO 5801 [3], the dynamic pressure at the system outlet is assumed to be lost so that

$$p_{t,dif,o} - p_{t,down} \approx \alpha_{edit} \rho v_{dif}^2 / 2 \quad (15)$$

which implies that $p_{s,dif,o} \approx p_{\infty}$.

Substituting equations (11) to (15) into equation (10) and rearranging yields the draught equation that was given in equation (1).

References

- [1] G. M. Bekker, C. J. Meyer and S. J. Van der Spuy. Numerical investigation of pressure recovery in an induced draught fan arrangement. *R & D Journal*. 36:19-28, 2020.
- [2] M. B. Wilkinson, S. J. Van der Spuy and T. W. Von Backström. The Design of a Large Diameter Axial Flow Fan for Air-Cooled Heat Exchanger Applications. In *ASME Turbo Expo 2017: Turbomachinery Technical Conference and Exposition*, Charlotte, NC, USA, 2017.
- [3] BS EN ISO 5801. *Industrial fans – Performance testing using standardized airways*. British Standard Institution, 2008.
- [4] G. M. Bekker, C. J. Meyer and S. J. Van der Spuy. Performance enhancement of an induced draught axial flow fan through pressure recovery. *R & D Journal*. 37:35-44, 2021.
- [5] D. G. Kröger. *Air-cooled heat exchangers and cooling towers: Thermal-flow performance evaluation and design*. Department of Mechanical Engineering, Matieland, 1998.
- [6] P. D. Clausen, S. G. Koh and D. H. Wood. Measurements of a swirling turbulent boundary layer developing in a conical diffuser. *Experimental Thermal and Fluid Science*. 6(1):39-48, 1993.
- [7] D. C. Wilcox. *Turbulence Modeling for CFD*. 2nd ed. DCW Industries, 1998.
- [8] M. B. Wilkinson. *The design of an axial flow fan for air-cooled heat exchanger applications*. Master’s Thesis, Department of Mechanical and Mechatronic Engineering, Stellenbosch University, 2017.
- [9] C. J. Greenshields. *OpenFOAM: User Guide*. 5th ed. OpenFOAM Foundation Ltd., 2017.
- [10] A. Terzis, I. Stylianou, A. I. Kalfas and P. Ott. Heat transfer and performance characteristics of axial cooling fans with downstream guide vanes. *Journal of Thermal Science*. 21(2):162-171, 2012.
- [11] D. C. Wilcox. Reassessment of the scale-determining equation for advanced turbulence models. *AIAA Journal*. 26(11):1299-1310, 1988.
- [12] S. J. Van der Spuy. *Perimeter fan performance in forced draught air-cooled steam condensers*. PhD Thesis, Department of Mechanical and Mechatronic Engineering, Stellenbosch University, 2011.
- [13] R. A. Engelbrecht. *Numerical investigation of fan performance in a forced draft air-cooled condenser*. PhD Thesis, Department of Mechanical and Mechatronic Engineering, Stellenbosch University, 2018.
- [14] F. G. Louw, P. R. P. Bruneau, T. W. Von Backström and S. J. Van der Spuy. The design of an axial flow fan for application in large air-cooled heat exchangers. In *ASME Turbo Expo 2012: Turbomachinery Technical Conference and Exposition*, Copenhagen, Denmark, 2012.
- [15] R. A. Wallis. *Axial flow fans and ducts*. John Wiley & Sons, 1983.
- [16] D. L. Louw, C. J. Meyer and S. J. Van der Spuy. Numerical investigation of an induced draft air-cooled condenser under crosswind conditions. In *ASME 2021 Summer Heat Transfer Conference*, June 16-18, Virtual conference, Online, 2021.
- [17] M. B. Wilkinson, S. J. Van der Spuy and T. W. Von Backström. Performance Testing of an Axial Flow Fan Designed for Air-Cooled Heat Exchanger Applications. In *ASME Turbo Expo 2018: Turbomachinery Technical Conference and Exposition*, Oslo, Norway, 2018.